RESEARCH ARTICLE SUMMARY

IMMUNE SIGNALING

Cyclic ADP ribose isomers: Production, chemical structures, and immune signaling

Mohammad K. Manik†, Yun Shi†, Sulin Li†, Mark A. Zaydman, Neha Damaraju, Samuel Eastman, Thomas G. Smith, Weixi Gu, Veronika Masic, Tamim Mosaiab, James S. Weagley, Steven J. Hancock, Eduardo Vasquez, Lauren Hartley-Tassell, Nestoras Kargios, Natsumi Maruta, Bryan Y. J. Lim, Hayden Burdett, Michael J. Landsberg, Mark A. Schembri, Ivan Prokes, Lijiang Song, Murray Grant, Aaron DiAntonio, Jeffrey D. Nanson, Ming Guo, Jeffrey Milbrandt, Thomas Ve*, Bostjan Kobe*

INTRODUCTION: Organisms from bacteria to animals and plants must defend themselves against pathogens. Homologous protein motifs exist in immune pathways of all organisms. One such motif is the TIR domain, named after the mammalian immune receptors—Toll-like receptors and interleukin-1 receptors—where it was first identified. Two properties are shared among most TIR domains from all organisms: the ability to self-associate and enzymatic activity involving the cleavage of nicotinamide adenine dinucleotide (oxidized form) (NAD^+). NAD^+ is a metabolite with redox properties that has roles in many cellular processes. In some cases, cleavage of NAD^+ leads to the production of cyclic adenosine monophosphate (ADP)–ribose (cADPR) isomers.

RATIONALE: In bacteria, NAD^+-cleavage activity by TIR domain–containing proteins plays a role in defense signaling, as well as suppression of host immunity. One corresponding pathway is termed the Thoeris defense system. This signaling pathway protects bacteria against phage infection and involves the *thsA* and *thsB* genes. Upon phage infection, ThsB (a TIR-domain protein) cleaves NAD^+ and produces a cADPR isomer, which activates ThsA-mediated killing of the infected cell, thus protecting the bacterial population. Another bacterial protein that produces a cADPR isomer is HopAM1, the TIR-domain effector protein from *Pseudomonas syringae* DC3000, which is involved in suppressing plant immunity. The chemical structures and mechanisms of action of the responsible cADPR isomers were unknown before this work. Our aim was to determine the chemical structures of cADPR isomers, the structural basis of their production by bacterial TIR domains, and their mechanism of action in Thoeris defense signaling and suppression of plant immunity.

RESULTS: Using a combination of methods, including nuclear magnetic resonance (NMR), mass spectrometry, and crystallography, we show that the cADPR isomers are cyclized by O-glycosidic bond formation between the ribose moieties in ADPR. Structures of TIR domains that produce cADPR isomers, as determined by crystallography and cryo–electron microscopy, reveal conformational changes that lead to an active assembly that resembles those of Toll-like receptor adaptor TIR domains. Mutagenesis reveals a conserved tryptophan that is essential for cyclization. Using crystallography and biophysical approaches, we show that one of the cADPR isomers (3′cADPR) is an activator of Thoeris ThsA proteins responsible for antiphage defense, by inducing a change in its tetrameric state. We also show that the same cADPR isomer is a suppressor of plant immunity when produced by the effector HopAM1.

CONCLUSION: Collectively, our results reveal the molecular basis of cADPR isomer production. The 2′cADPR and 3′cADPR differ only in the location of the O-glycosidic bond between the ribose moieties in ADPR. These compounds add to the growing list of signaling molecules identified in immune pathways that involve proteins containing TIR domains and may represent intermediates in their synthesis or signaling molecules with their own distinctive activities. Our results establish the 3′cADPR isomer produced by bacterial TIR domain–containing proteins as an antiviral and plant immunity–suppressing signaling molecule. ■

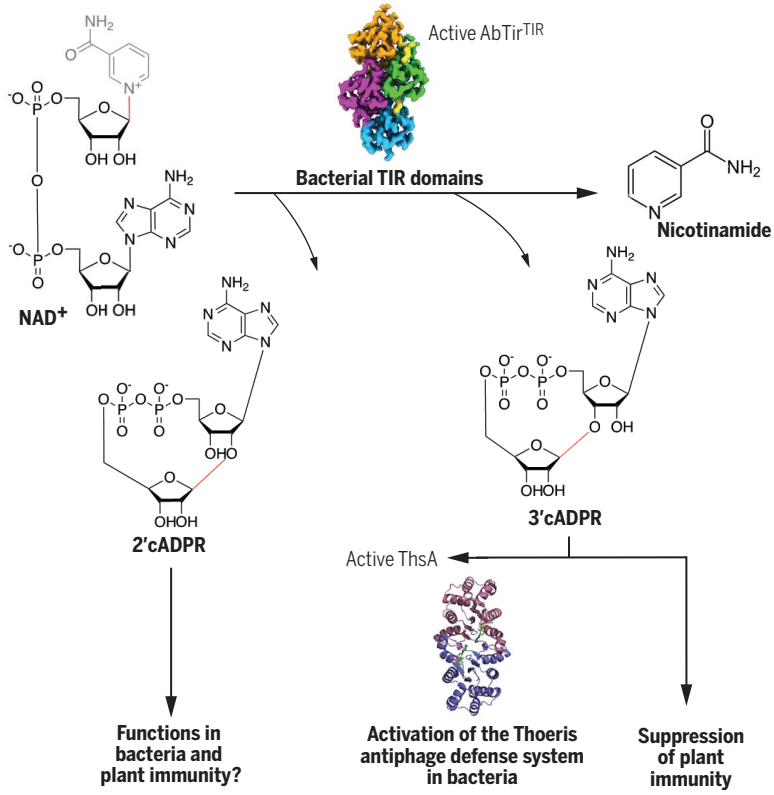

Diverse immune roles of bacterial cADPR isomers. Bacteria have TIR domain–containing proteins that cleave NAD to produce cyclic ADPR isomers with different cyclic linkages. One of these molecules, 3′cADPR, has roles in diverse immunity pathways. It acts as an activator of the Thoeris antiphage defense system by binding to the protein ThsA. When produced by the effector HopAM1 from the plant pathogen *P. syringae*, it suppresses plant immunity.

The list of author affiliations is available in the full article online.
*Corresponding author. Email: b.kobe@uq.edu.au (B.K.); t.ve@griffith.edu.au (T.V.)
†These authors contributed equally to this work.
Cite this article as M. K. Manik *et al.*, *Science* **377**, eadc8969 (2022). DOI: 10.1126/science.adc8969

READ THE FULL ARTICLE AT
https://doi.org/10.1126/science.adc8969

RESEARCH ARTICLE

IMMUNE SIGNALING

Cyclic ADP ribose isomers: Production, chemical structures, and immune signaling

Mohammad K. Manik[1,2]†‡§, Yun Shi[3]†, Sulin Li[1,2]†, Mark A. Zaydman[4], Neha Damaraju[5,6], Samuel Eastman[7], Thomas G. Smith[8]¶, Weixi Gu[1,2], Veronika Masic[3], Tamim Mosaiab[3], James S. Weagley[9], Steven J. Hancock[1,2]#, Eduardo Vasquez[3], Lauren Hartley-Tassell[3], Nestoras Kargios[10], Natsumi Maruta[1,2], Bryan Y. J. Lim[1,2], Hayden Burdett[1,2]**, Michael J. Landsberg[1,2], Mark A. Schembri[1,2], Ivan Prokes[11], Lijiang Song[11], Murray Grant[10], Aaron DiAntonio[4,5], Jeffrey D. Nanson[1,2], Ming Guo[12], Jeffrey Milbrandt[4], Thomas Ve[3]*, Bostjan Kobe[1,2,13]*

Cyclic adenosine diphosphate (ADP)–ribose (cADPR) isomers are signaling molecules produced by bacterial and plant Toll/interleukin-1 receptor (TIR) domains via nicotinamide adenine dinucleotide (oxidized form) (NAD^+) hydrolysis. We show that v-cADPR (2′cADPR) and v2-cADPR (3′cADPR) isomers are cyclized by O-glycosidic bond formation between the ribose moieties in ADPR. Structures of 2′cADPR-producing TIR domains reveal conformational changes that lead to an active assembly that resembles those of Toll-like receptor adaptor TIR domains. Mutagenesis reveals a conserved tryptophan that is essential for cyclization. We show that 3′cADPR is an activator of ThsA effector proteins from the bacterial antiphage defense system termed Thoeris and a suppressor of plant immunity when produced by the effector HopAM1. Collectively, our results reveal the molecular basis of cADPR isomer production and establish 3′cADPR in bacteria as an antiviral and plant immunity–suppressing signaling molecule.

The ~150-residue Toll/interleukin-1 receptor (TIR) domains are widely distributed in animals, plants, and bacteria and function through self-association and homotypic interactions with other TIR domains (*1*). In plants and animals, these domains are predominantly found in proteins with immune functions [Toll-like receptors (TLRs), interleukin-1 receptors (IL-1Rs), and their adaptor proteins] (*2*) and plant nucleotide-binding, leucine-rich repeat receptors (NLRs) (*3*, *4*). TIR domains form higher-order oligomers and orchestrate signal amplification by a mechanism called signaling by cooperative assembly formation (SCAF) (*3*, *5*–*7*).

In bacteria, initial studies suggested that TIR domain–containing proteins, such as TcpB, TcpC, TirS, PumA, and TcpS, serve as virulence factors that inhibit host innate immune signaling by molecular mimicry, although it is not clear how they enter the cell (*8*). Bacterial TIR domain–containing proteins are further implicated in antiphage defense systems (*9*–*12*).

Many TIR domains have been found to cleave nicotinamide adenine dinucleotide (oxidized form) (NAD^+) (*13*–*16*). In animals, SARM1 (sterile alpha and Toll/interleukin-1 receptor motif-containing 1) is a metabolic sensor of axonal nicotinamide mononucleotide (NMN) and NAD^+ levels, and its TIR domain executes programmed axon death by cleaving NAD^+ into nicotinamide and either adenosine diphosphate (ADP)–ribose (ADPR) or cyclic ADPR (cADPR) (*13*, *16*, *17*). The TIR domains of plant NLRs (TNLs) similarly cleave NAD^+ into nicotinamide and either ADPR or a cADPR isomer known as variant cADPR (v-cADPR) (*14*), which has a different but unknown cyclization site compared with canonical cADPR (*18*). A conserved catalytic glutamate is required for NAD^+ hydrolysis by SARM1 and plant TIR domains, and the same glutamate is required for SARM1 to trigger axon degeneration and plant TNLs to trigger a localized cell death in response to infections (*13*, *14*, *16*). v-cADPR is a biomarker of plant TNL enzymatic activity but may not be sufficient in and of itself to trigger a cell-death response (*19*).

Bacterial TIR domains can also cleave NAD^+ (*10*, *15*, *20*–*22*), again producing nicotinamide and ADPR or the distinct cADPR isomers v-cADPR or v2-cADPR. In bacteria, NAD nucleosidase (NADase) activity by TIR domains is a critical component of STING cyclic dinucleotide sensing (*10*) and the Thoeris defense system (*9*). The Thoeris system protects bacteria against phage infection and consists of two genes: *thsA* and *thsB* (the latter can be present in one or multiple copies). The *thsA* gene encodes a protein that contains either an N-terminal SIR2-like (silent information regulator 2) domain and a C-terminal SLOG-like domain (from the superfamily of ribonuclease like proteins named after SMF/DprA and LOG proteins) or a multitransmembrane N-terminal domain with a C-terminal macro domain. SIR2 domains hydrolyze NAD^+, whereas SLOG domains can bind to NAD^+-derived metabolites and have been suggested as sensors for nucleotide-related ligands (*9*, *23*). The *thsB* gene encodes a TIR domain–containing protein (ThsB) (*9*, *22*–*24*). Upon phage infection, ThsB cleaves NAD^+ and produces a cADPR isomer, which activates ThsA (*22*), causing further NAD^+ depletion and cell death. HopAM1, a bacterial TIR-domain effector protein from *Pseudomonas syringae* DC3000, suppresses plant immunity by producing v2-cADPR (*21*).

TIR domain self-association is required for the NADase activity of SARM1 as well as plant TNLs (*13*, *16*). Crystal and cryo–electron microscopy (cryo-EM) structures of SARM1 in its active conformation revealed the active site spanning two TIR-domain molecules, explaining the requirement for self-association (*25*). The architectures of oligomeric assemblies formed by plant and SARM1 TIR domains are similar ("enzyme assemblies") but are distinct from those formed by animal TIR domains involved in TLR signaling ("scaffold assemblies") [reviewed in (*3*)]. Both types of assemblies feature open-ended complexes with two strands of TIR domains in a head-to-tail arrangement but differ in the orientation of the two strands (antiparallel in enzyme assemblies, parallel in scaffold assemblies). Some plant TIR domains have also been shown to act as 2′,3′-cAMP and 2′,3′-cGMP synthetases, by hydrolyzing RNA and DNA, which requires a different TIR-domain oligomeric architecture

[1]School of Chemistry and Molecular Biosciences, The University of Queensland, Brisbane, QLD 4072, Australia. [2]Australian Infectious Diseases Research Centre, The University of Queensland, Brisbane, QLD 4072, Australia. [3]Institute for Glycomics, Griffith University, Southport, QLD 4222, Australia. [4]Department of Pathology and Immunology, Washington University School of Medicine in St. Louis, St. Louis, MO 63100, USA. [5]Department of Developmental Biology, Washington University School of Medicine in St. Louis, St. Louis, MO 63100, USA. [6]Department of Genetics, Washington University School of Medicine in St. Louis, St. Louis, MO 63100, USA. [7]Department of Plant Pathology, University of Nebraska–Lincoln, Lincoln, NE 68583, USA. [8]Department of Chemistry, University of Nebraska–Lincoln, Lincoln, NE 68588, USA. [9]Edison Family Center for Genome Sciences and Systems Biology, Washington University School of Medicine in St. Louis, St. Louis, MO 63110, USA. [10]School of Life Sciences, University of Warwick, Coventry CV4 7AL, UK. [11]Department of Chemistry, University of Warwick, Coventry CV4 7AL, UK. [12]Department of Agronomy and Horticulture, University of Nebraska–Lincoln, Lincoln, NE 68583, USA. [13]The University of Queensland, Institute for Molecular Bioscience, Brisbane, QLD 4072, Australia.
***Corresponding author. Email: b.kobe@uq.edu.au (B.K.); t.ve@griffith.edu.au (T.V.)**
†These authors contributed equally to this work.
‡Present address: Department of Biological Chemistry and Molecular Pharmacology, Harvard Medical School, Boston, MA 02115, USA.
§Present address: Program in Cellular and Molecular Medicine, Boston Children's Hospital, Boston, MA 02115, USA.
¶Present address: Department of Chemistry, University of Minnesota, Minneapolis, MN 55455, USA.
#Present address: Wellcome Wolfson Institute for Experimental Medicine, School of Medicine, Dentistry and Biomedical Sciences, Queen's University Belfast, Belfast BT12 6BA, UK.
**Present address: Wellcome Centre for Cell Biology, University of Edinburgh, Edinburgh EH9 3BF, UK.

(*26*) (cAMP, cyclic adenosine monophosphate; cGMP, cyclic guanosine monophosphate). A limited number of bacterial TIR domains have been characterized structurally and functionally (*23*, *27*–*30*). In this study, we characterized the cyclization site of cADPR isomers, the molecular basis of their production by TIR domains, and their functions in immunity pathways in bacteria and plants.

O-glycosidic linkage between ribose sugars in cADPR isomers

To identify the sites of cyclization in cADPR isomers, we expressed and purified the TIR domains of AbTir (from *Acinetobacter baumannii*; AbTir^{TIR}) and a protein from *Aquimarina amphilecti* (AaTir^{TIR}; fig. S1A and table S1), which produce v- and v2-cADPR, respectively (*15*, *31*). Comparative genomics analyses suggest that AbTir has functions distinct from the Thoeris defense system (fig. S1B).

Real-time nuclear magnetic resonance (NMR)–based and fluorescence-based NADase assays confirmed that purified AbTir^{TIR} and AaTir^{TIR} are enzymatically active and produce cADPR isomers (Fig. 1A and fig. S1, C and D). AbTir^{TIR}-produced v-cADPR is identical to the cADPR isomer produced by TIR domains of the plant immune receptors L6 and ROQ1 (Fig. 1A). Both AbTir^{TIR} and AaTir^{TIR} can catalyze base-exchange reactions with 8-amino-isoquinoline (fig. S2A). They can also use nicotinamide adenine dinucleotide phosphate (NADP$^+$) as a substrate, but its cleavage only yields nicotinamide and adenosine diphosphate ribose 2′-phosphate (ADPPR), indicating that cADPR-isomer production is specific to NAD$^+$ cleavage (fig. S2B). We also tested the activities in the presence of NAD$^+$, adenosine triphosphate (ATP), and Mg^{2+} and observed no formation of metabolites reported for plant TIR domains (*32*, *33*) (fig. S1F).

We purified v-cADPR and v2-cADPR from the reaction mixture, using high-performance liquid chromatography (HPLC), and determined their chemical structures using NMR (Fig. 1B; figs. S1E and S2, C to D; and tables S2 and S3). The heteronuclear multiple bond correlation (HMBC) NMR spectrum of AbTir^{TIR}-produced v-cADPR shows both H1″-C2′ and H2′-C1″ cross-peaks, revealing that AbTir^{TIR} catalyzes the formation of a ribose(1″→2′)ribose O-glycosidic linkage in ADPR (Fig. 1B). By contrast, the HMBC spectrum of v2-cADPR, produced by AaTir^{TIR}, shows both H1″-C3′ and H3′-C1″ cross-peaks, indicating that AaTir^{TIR} catalyzes the formation of a ribose(1″→3′)ribose O-glycosidic linkage in ADPR (Fig. 1, B and C). Because the β configuration of the anomeric carbon in NAD$^+$ is retained in AbTir^{TIR} and

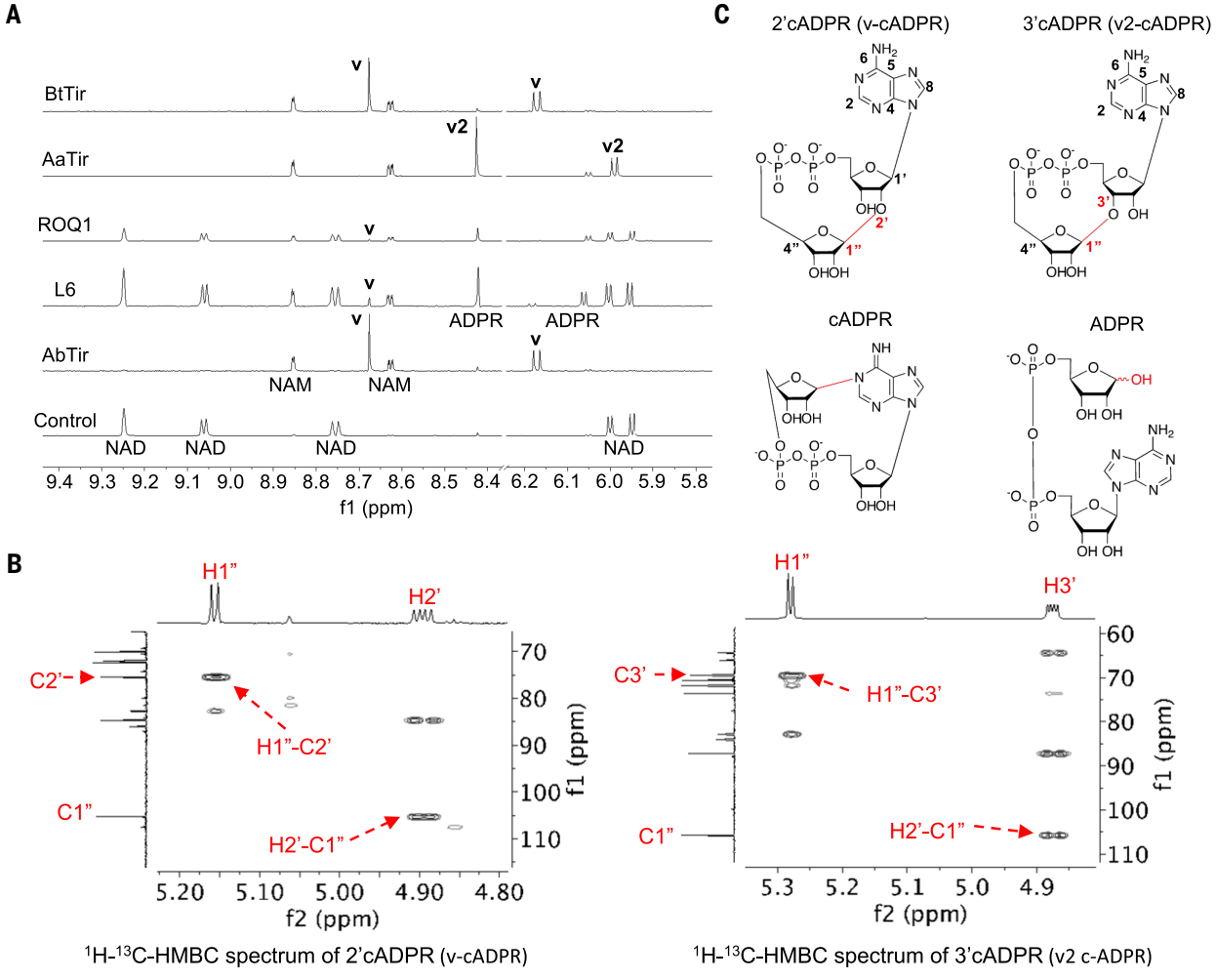

^{1}H-^{13}C-HMBC spectrum of 2′cADPR (v-cADPR)

^{1}H-^{13}C-HMBC spectrum of 3′cADPR (v2 c-ADPR)

Fig. 1. Chemical structures of v- and v2-cADPR. (**A**) Expansions of ^{1}H NMR spectra showing NADase reactions by 0.1 μM AbTir^{TIR} (*A. baumannii*), 100 μM L6^{TIR} (flax), 26 μM ROQ1^{TIR} (*N. benthamiana*), 0.5 μM AaTir^{TIR} (*A. amphilecti*), and 2.5 μM BtTir^{TIR} (*B. thetaiotaomicron*; table S1). The initial concentration for NAD$^+$ was 500 μM, except for L6 (1 mM). Spectra correspond to 16 hours of incubation time, except for ROQ1 (incubation time of 64 hours). Selected peaks are labeled, showing the formation v-cADPR (v) and v2-cADPR (v2). (**B**) Expansions of HMBC spectra showing correlations through glycosidic linkages for 2′cADPR (v-cADPR) and 3′cADPR (v2-cADPR). ppm, parts per million. (**C**) Chemical structures of 2′cADPR, 3′cADPR, cADPR, and ADPR. Important NMR peaks (B) and their correlated positions in the chemical structure (C) are labeled, showing a 1″-2′ linkage for v-cADPR and a 1″-3′ linkage for v2-cADPR.

AaTir^{TIR}-catalyzed base-exchange reactions (fig. S2A) and the coupling constants of the anomeric protons of v-cADPR (J1″,2″ ~ 5.0 Hz) and v2-cADPR (J1″,3″ ~ 4.4 Hz) are similar to those of NAD$^+$ (5 to 6 Hz), both cADPR isomers are likely to retain the same β configuration. v2-cADPR purified from *Nicotiana benthamiana* leaves expressing HopAM1 showed an identical chemical structure to that of AaTir^{TIR} (table S4). Based on these chemical structures, we term these molecules 2′cADPR and 3′cADPR, highlighting the linkages between ribose rings of v-cADPR and v2-cADPR, respectively.

Ligand-free structures and self-association of bacterial TIR domains

SARM1 and plant TIR domains require self-association for their NADase activity (*13*, *25*, *34*, *35*). The NADase activity of AbTir^{TIR} increases disproportionally with increasing protein concentrations and increases in the presence of molecular crowding agents (fig. S3, A and B). Size-exclusion chromatography coupled with multiangle light scattering (SEC-MALS) experiments show that AbTir self-associates in a concentration-dependent manner (fig. S3, C and D), which requires both the TIR domain and the N-terminal coiled coil (CC) domain (AbTir^{CC}). AbTir$^{full\text{-}length}$ shows an initially suppressed enzymatic activity, suggesting that conformational rearrangements are required for efficient NAD$^+$ cleavage (fig. S1C). Taken together, these results suggest that cADPR isomer–producing bacterial TIR domains also require self-association for their NADase activity.

To provide insight into the molecular basis of cADPR isomer production by TIR domains, we determined the crystal structures of AbTir^{TIR} and a closely related v-cADPR (2′cADPR)–producing TIR domain protein (47% sequence identity) from *Bacteroides thetaiotaomicron* (residues 156 to 287; BtTir^{TIR}; Fig. 1, figs. S1A and S2A, and table S1), at 2.16- and 1.42-Å resolution, respectively (fig. S4, A and B, and table S5). The structure of AbTir^{TIR} closely resembles the structures of BtTir^{TIR}, PdTir^{TIR} [Protein Data Bank (PDB) ID 3H16], and the v-cADPR (2′cADPR)–producing TcpB^{TIR} (PDB ID 4C7M) (*27*–*30*), with Cα root mean square distance (RMSD) values of 1.2, 1.8, and 1.9 Å, respectively (fig. S4, B and C). Both AbTir^{TIR} and BtTir^{TIR} show less similarity to the cADPR isomer–producing ThsB TIR domain of the *Bacillus cereus* MSX-D12 Thoeris defense system (BcThsB; PDB ID 6LHY; Cα RMSD values of 4.4 and 2.5 Å for AbTir^{TIR} and BtTir^{TIR}, respectively).

In TIR domains with NADase activity (from SARM1; plant TNLs RPP1, ROQ1, and RUN1; and oyster TIR-STING; table S1), the conserved glutamate residue essential for NADase activity is localized in a pocket consisting of residues from the βA strand, the AA and BB loops, and the αB and αC helices (*10*, *13*, *25*, *34*). In AbTir^{TIR} and BtTir^{TIR}, the αB and αC helices adopt different conformations and the equivalent glutamate residue (E208 in AbTir; E230 in BtTir) is surface exposed (fig. S4D). Comparing the different chains in the asymmetric unit of the AbTir^{TIR} crystal, the region around E208 is highly flexible. Crystal packing of AbTir^{TIR} and BtTir^{TIR} reveals a common symmetric interface (figs. S4C and S5A), with a large buried surface area (BSA) (AbTir^{TIR}, 1875 Å^2; BtTir^{TIR}, 1332 Å^2), which is also observed in the crystals of PdTir^{TIR} and TcpB^{TIR} (fig. S5A and table S1). The structures suggest that they represent an inactive conformation, possibly stabilized by the symmetric dimeric arrangement.

Cryo-EM structure of AbTir^{TIR} bound to NAD$^+$ mimic

We reasoned that we could capture the active state of AbTir by using base-exchange products of NAD$^+$ hydrolysis, which are more biochemically stable than NAD$^+$ itself and could resist cleavage at high concentrations of the enzyme (*25*). Indeed, in the presence of 8-amino-isoquinoline adenine dinucleotide (3AD), we could visualize filamentous structures of AbTir^{TIR} by negative-stain electron microscopy (Fig. 2A). Filaments could be observed in the presence of NAD$^+$, but too few to support structure determination (fig. S6A). We determined the cryo-EM structure of AbTir^{TIR}:3AD filaments at 2.74-Å resolution (fig. S6 and table S6), which shows the presence of 3AD molecules between monomers of AbTir^{TIR} and an arrangement of TIR domains different from the enzyme assemblies of SARM1 and plant TIR domains but analogous to the scaffold assemblies of the TLR adaptor proteins MAL and MyD88, each of which contains two parallel strands of TIR domains arranged head to tail (Fig. 2, B and D, and fig. S5B) (*3*). The intrastrand "BE" interface (BSA of 710 Å^2) involves the BB-loop, whereas the interstrand "BCD" interface involves one molecule interacting with two molecules in the parallel strand (BSAs of 1340 and 1410 Å^2, respectively). Assembly formation is accompanied by conformational changes involving the BB-loop and the αB and αC helices (RMSD of 1.8 Å for 101 Cα atoms; Fig. 2C and movie S1). The BB-loop and αB helix have tilted outward by ~50° to 55°, whereas the αC helix has refolded and includes residues from both the CC and CD loops. Because it is arranged through the analogous BE interface, the AbTir^{TIR} active site is very similar to that of SARM1^{TIR}, including the conformation of the 3AD molecule (Fig. 2E). Using site-directed mutagenesis, we verified the importance of residues in both the active-site region and in the inter- and intrastrand interfaces for NADase activity of AbTir^{TIR} (Fig. 3A, fig. S7, and table S7).

Tryptophan affects ADPR cyclization

The products of the NADase reaction were also assessed for the AbTir mutants (table S7). The analysis revealed that only the W204A (Trp^{204}→Ala) mutant has reduced production of v-cADPR (2′cADPR) compared with wild-type AbTir, demonstrating its importance for ADPR cyclization (Fig. 3B, fig. S8A, and table S7). We tested whether the mutation of the equivalent tryptophan residue has a similar effect on ADPR cyclization by other bacterial TIR domain–containing proteins. We analyzed the conservation of W204 in a multiple sequence alignment of 122 TIR domains (*15*, *16*, *31*). We observed conservation of aromatic residues at this position among all TIR domains that produced a cyclic ADPR product [cADPR, v-cADPR (2′cADPR), or v2-cADPR (3′cADPR)] in vitro, with a strong preference for tryptophan—W (9 of 12), Y (Tyr) (2 of 12), and F (Phe) (1 of 12) (fig. S8B). This conservation is weaker among TIR domains that either produce noncyclic products (nicotinamide and ADPR) or lack activity altogether in vitro. These observations suggest that a large aromatic residue at this position facilitates the production of a cyclic ADPR product.

To further identify positions important for determining the product specificity of TIR-domain NADases, we analyzed 278 TIR-domain sequences and confirmed that the position corresponding to the tryptophan differs between cyclase and noncyclase TIR domains, although not among cyclase TIR domains that produce different forms of cADPR (data S1 to S4). All cyclase TIR domains contain an aromatic residue at this position (fig. S9, A to E).

We tested the functional importance of the conserved aromatic residue by performing site-directed mutagenesis on TIR domains known to produce different products (fig. S8, C and D), with conservative (W, Y, or F) or disruptive (A) mutations. Reaction products were analyzed by HPLC (fig. S8, C and D). For all TIR domains that produce a cyclic product, the mutants exhibited a decrease in cyclic product formation and an increase in ADPR when compared with the wild-type proteins (Fig. 3, C to F). The nonconservative alanine mutations typically exhibited the greatest impact on the relative production of a cyclic product versus ADPR; however, this trend was not universally true. Mutations in the background of an ADPR-producing template had variable impacts on NADase activity (fig. S8E), but ADPR always remained the only catabolite produced. These results are consistent with the conclusion that the position equivalent to W204 in AbTir is critical for the production of cyclic ADPR products.

3′cADPR (v2-cADPR) activates Thoeris ThsA

Bacterial lysates containing cADPR isomers produced by bacterial ThsB or plant TIR domains have been shown to activate the ThsA NADase (Fig. 4A) of the *B. cereus* MSX-D12 Thoeris antiphage defense system (*22*). To test

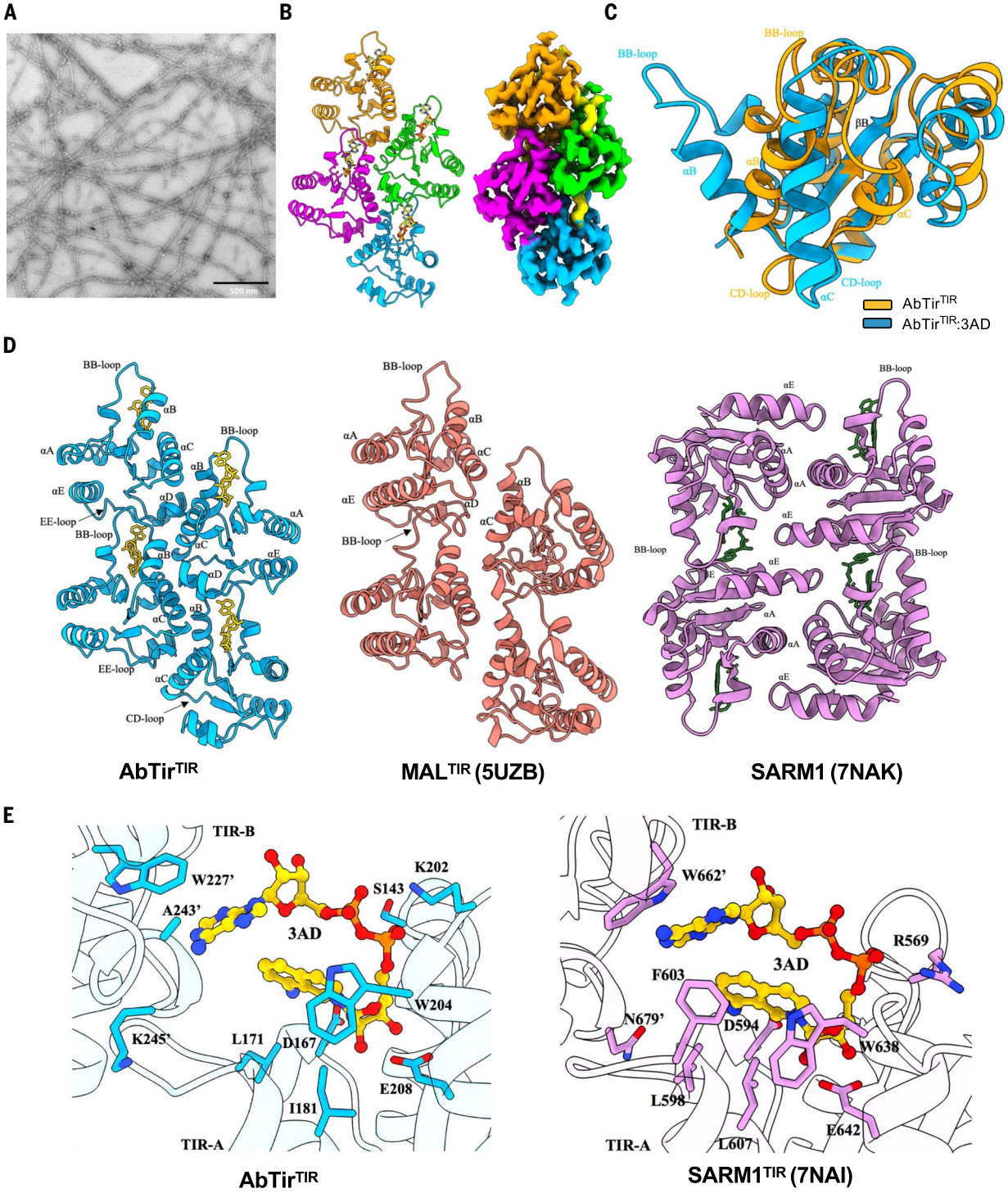

Fig. 2. Cryo-EM structure of the AbTir^{TIR}:3AD filament. (**A**) Negative-stain electron micrograph of AbTir^{TIR}:3AD filaments. (**B**) Cartoon representation and electrostatic potential density map of the AbTir^{TIR}:3AD filament. TIR domain subunits are shown in blue, green, magenta, and orange. 3AD is shown in yellow. (**C**) Structural superposition of ligand-free (crystal structure, orange) and 3AD-bound AbTir^{TIR} (cryo-EM structure, cyan) molecules reveal conformational changes in the BB-loop and αB and αC helices upon substrate binding. (**D**) Comparison of AbTir^{TIR}:3AD, MAL^{TIR} (PDB ID 5UZB) and SARM1^{TIR}:1AD (PDB ID 7NAK) assemblies. (**E**) Comparison of the active sites in AbTir^{TIR} and SARM1^{TIR} (PDB ID 7NAI) reveals similar substrate-binding modes.

if our purified cADPR isomers can directly activate ThsA, we produced and purified four different ThsA proteins (37 to 46% sequence identity) from *B. cereus* MSX-D12 (BcThsA), *A. baumannii* (AbThsA), *Enterococcus faecium* (EfThsA), and *Streptococcus equi* (SeThsA) and monitored the NAD^+-cleavage activity of each in the absence and presence of ADPR, cADPR, v-cADPR (2′cADPR), and v2-cADPR (3′cADPR) using our NMR-based NADase assay (Fig. 4, B and C, and fig. S10, A and B). AbThsA, BcThsA, and a SIR2 domain–only construct of BcThsA (BcThsA^{SIR2}) cleave NAD^+ (fig. S10, A to C), whereas EfThsA, SeThsA, and SeThsA^{SIR2} (Fig. 4, B and C, and fig. S10C) are almost inactive under

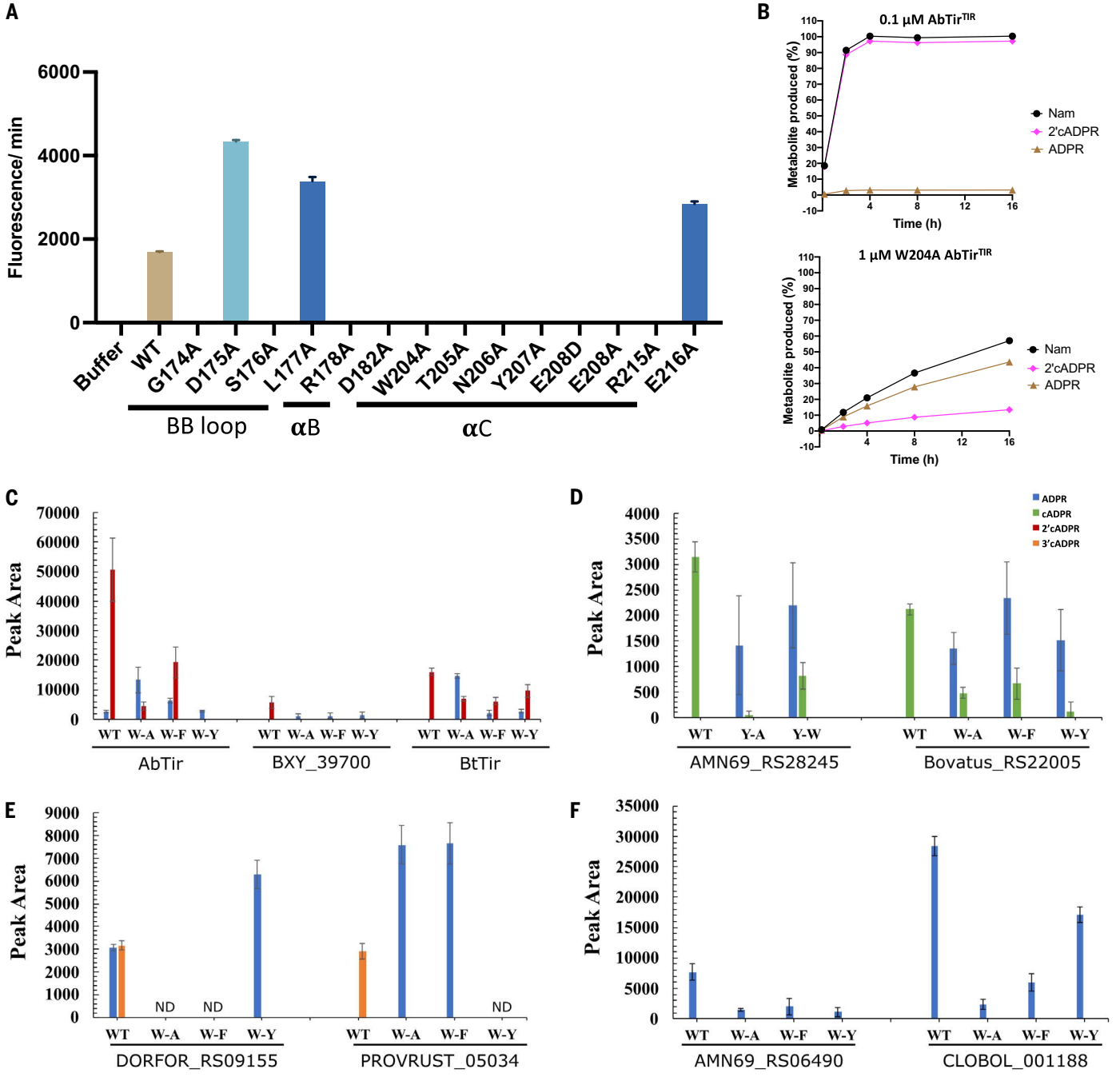

Fig. 3. Mutagenesis of bacterial TIR domains. (**A**) NADase activity of AbTir^{TIR} mutants, using the fluorescence-based assay, with 100 μM εNAD and 100 μM protein. Data are presented as means ± SD (n = 3). (**B**) Production of 2′cADPR and ADPR by wild-type AbTir^{TIR} and its W204A mutant, monitored by ^{1}H NMR, using an initial NAD^{+} concentration of 500 μM. (**C** to **F**) Mutations of the position equivalent to AbTir W204 affect the production of cyclic NAD^{+} catabolites by TIR domains (table S1). The NAD^{+} catabolite peak areas for wild-type and mutant TIR domain reactions after 1 hour are shown. TIR domain grouping is based on the primary product of the wild-type protein [n = 3 for all groups except where no data (ND) could be collected; data are presented as means ± SD].

the same conditions (less than 10% of NAD^{+} consumed after 40 hours). Neither BcThsA nor AbThsA are further activated by ADPR, cADPR, v-cADPR (2′cADPR), or v2-cADPR (3′cADPR) (fig. S10B), suggesting that they have been produced in a fully activated state. Both autoactive and inactive versions of ligand-free BcThsA have previously been reported (*22*, *23*), suggesting that the inactive states of some ThsA variants are sensitive to the choice of purification method or tag. EfThsA and SeThsA cleave NAD^{+} in the presence of 500 μM v-cADPR (2′cADPR) or v2-cADPR (3′cADPR) (Fig. 4, B and C). A dose-response is observed with v2-cADPR (3′cADPR) treatment, and both proteins are activated by v2-cADPR (3′cADPR) concentrations as low as 5 μM (Fig. 4C). In comparison, v-cADPR (2′cADPR) only activates these proteins at the highest concentration tested (500 μM). ADPR and cADPR have no effect on the NADase activity of EfThsA and SeThsA (Fig. 4B).

Isothermal titration calorimetry (ITC) measurements showed that v2-cADPR (3′cADPR) binds directly to inactive (EfThsA) and autoactive (AbThsA) forms of ThsA at a ~1:1 molar ratio, with dissociation constant (K_d)

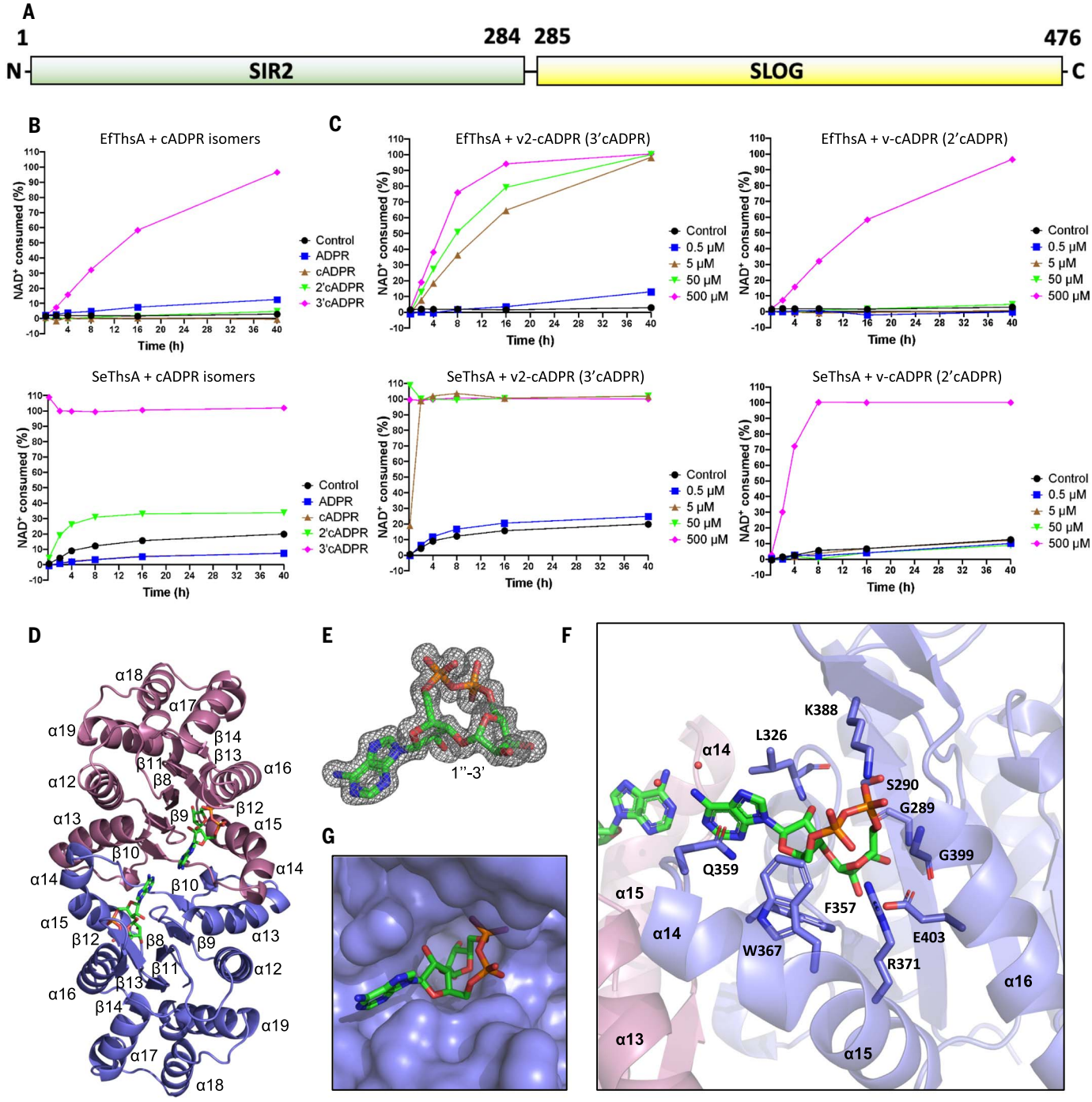

Fig. 4. Binding of v2-cADPR (3′cADPR) to ThsA^{SLOG}. (**A**) Schematic diagram of ThsA domain organization. Residue numbering corresponds to BcThsA (domain boundaries: BcThsA-SIR2, 1 to 283; SLOG, 284 to 476). AbThsA, EfThsA, and SeThsA have identical domain organizations. (**B**) Activation of EfThsA (0.5 μM) and SeThsA (10 μM) NADase activity by 500 μM ADPR, cADPR, v-cADPR (2′cADPR), and v2-cADPR (3′cADPR). The initial NAD^+ concentration was 500 μM. (**C**) Activation of EfThsA (0.5 μM) and SeThsA (10 μM) NADase activity by 0.5, 5, 50, and 500 μM v-cADPR (2′cADPR) and v2-cADPR (3′cADPR). The initial NAD^+ concentration was 500 μM. (**D**) Crystal structure of BcThsA^{SLOG} dimer (cartoon; chains colored in slate and magenta) in complex with v2-cADPR (3′cADPR) (green stick representation). (**E**) Standard omit mFo-DFc map of v2-cADPR (3′cADPR), contoured at 3.0 σ. (**F**) Enlarged cutaway of the v2-cADPR (3′cADPR) binding pocket in the BcThsA^{SLOG} structure. (**G**) Surface representation of the v2-cADPR (3′cADPR) binding pocket.

values of 59.1 ± 15.8 and 189 ± 1.6 nM, respectively (fig. S10, D and E). No binding was detected for v-cADPR (2′cADPR) using ITC (fig. S10, D and E), and the weaker binding affinity of v-cADPR (2′cADPR) was also corroborated by competition binding assays through saturation-transfer difference (STD) NMR, because v2-cADPR (3′cADPR) reduced v-cADPR (2′cADPR) binding to EfThsA, SeThsA, BcThsA, and AbThsA at an equal concentration (fig. S10F). Taken together, these findings support the model that ThsA is activated by TIR domain–produced cADPR isomers, with a preference for v2-cADPR (3′cADPR) over v-cADPR (2′cADPR).

3′cADPR (v2-cADPR) binds to the ThsA SLOG domain

To provide structural insights into cADPR isomer selectivity by ThsA, we determined the crystal structure of the SLOG domain of BcThsA ($BcThsA^{SLOG}$) in complex with v2-cADPR (3′cADPR) at 1.6-Å resolution (Fig. 4D and table S5). Continuous electron density for a cADPR isomer with a ribose(1″→3′)ribose O-glycosidic linkage was observed, confirming the structural configuration assigned by our NMR assays (Fig. 4E). $BcThsA^{SLOG}$ exists as a stable dimer in solution (fig. S11 and table S8) and forms a symmetric dimer (SLOG dimer) in the crystal, with an identical interface to the dimer observed in the ligand-free BcThsA structure (Fig. 4D and fig. S12A; PDB ID 6LHX) (*23*). Binding of v2-cADPR (3′cADPR) does not lead to substantial structural rearrangements in either the SLOG domain or the dimer interface (fig. S12A). 3′cADPR (v2-cADPR) binds to a highly conserved pocket adjacent to the symmetric dimer interface, and the adenine bases of the two v2-cADPR (3′cADPR) molecules in the dimer are only separated by 4.5 Å and are bridged by two water molecules (Fig. 4F, fig. S12B, and table S9). The C-2 and C-3 hydroxyls of the distal ribose interact with E403, whereas the diphosphate group is involved in hydrogen-bonding interactions with S290, R371, K388, and the backbone amide and carbonyl of G289 and G399, respectively (S, Ser; R, Arg; K, Lys; G, Gly). The adenine base stacks against the side chains of L326 and Q359, whereas the C-2 hydroxyl of the adenine-linked ribose forms a hydrogen bond with the backbone amide of L326 (Q, Gln). 2′cADPR (v-cADPR), which has a ribose(1″→2′)ribose O-glycosidic linkage, cannot form this latter hydrogen bond, and the adenosine moiety of this cADPR isomer is also likely to encounter steric hindrance with binding-pocket residues (Fig. 4G), explaining the preference for 3′cADPR. Mutational analysis confirmed the role of the structure-defined binding-pocket residues in ThsA activation (fig. S10G).

3′cADPR (v2-cADPR) changes ThsA tetramer organization

AbThsA, BcThsA, EfThsA, and SeThsA exist as tetramers in solution, and activation of SeThsA by v2-cADPR (3′cADPR) does not lead to a change in its oligomeric state (fig. S11 and table S8). However, the inactive $SeThsA^{SIR2}$ exists as a dimer in solution, whereas the fully active $BcThsA^{SIR2}$ exists as a monomer, suggesting that destabilization of SIR2:SIR2 domain interactions within the tetramer may be required for triggering the ThsA NADase activity (figs. S10C and S11 and table S8). To provide more detailed insight into how ThsA is activated by v2-cADPR (3′cADPR), we determined the ligand-free crystal structure of inactive SeThsA at 3.4-Å resolution (table S5) and compared it with the crystal structures of autoactive BcThsA (PDB ID 6LHX) (*23*) and our $BcThsA^{SLOG}$:v2-cADPR (3′cADPR) complex. Crystal-packing analyses reveal a D2 symmetric tetramer with a core consisting of two SIR2 dimers flanked by SLOG dimers at both sides (Fig. 5A). Both SIR2 dimer interfaces involve residues from the α3, α7, α9, and α10 helices. The crystal structure of autoactive BcThsA (PDB ID 6LHX) (*23*) has a tetramer with an identical architecture to SeThsA, but there are differences in the SIR2:SIR2 interfaces (Fig. 5, A and B). One of the molecules in the BcThsA SIR2 dimers has undergone a rotation of ~27° and translation of ~14 Å, compared with the SeThsA SIR2 dimers (Fig. 5C), resulting in a decrease of the interface area (2901.8 $Å^2$ in SeThsA; 1334.8 $Å^2$ in BcThsA). The α3 helix, which is involved in SIR2 dimerization but also covers a part of the predicted active site region in SeThsA (Fig. 5, B and D), adopts a different conformation ($SIR2^A$ and $SIR2^D$) or is disordered ($SIR2^B$ and $SIR2^C$) in BcThsA, enabling better access to catalytic residues (N113 and H153 in SeThsA, and N112 and H152 in BcThsA; N, Asn; H, His) (Fig. 5, B and D) (*23*). Comparison of the SLOG dimers in the inactive SeThsA structure with the dimer in the $BcThsA^{SLOG}$:v2-cADPR (3′cADPR) complex reveals that v2-cADPR (3′cADPR) binding is likely to induce changes in the orientation and position of the two SLOG domains (Fig. 5, E and F, and movie S2). In the SeThsA tetramer, this change will most likely cause the $SIR2^A$ and $SIR2^B$ domains and the $SIR2^C$ and $SIR2^D$ domains to move in opposite directions, bringing the α10 helices into closer proximity (Fig. 5G and movie S3), adopting a similar configuration to the SIR2 dimer interface observed in the crystal structure of autoactive BcThsA (Fig. 5B). We predict that this movement of the SIR2 domains is sufficient to destabilize the α3 helix conformation, enabling NAD^+ to access the active sites. SeThsA double mutants with reverse-charge substitutions of highly conserved residues in the SIR2 dimer interface (fig. S12C) are either autoactive (E170R, D251R; D, Asp) or not activated by v2-cADPR (3′cADPR) (R166E, R254E), confirming the role of the SIR2 dimer interface in regulating ThsA NADase activity (Fig. 5H). In summary, these findings reveal the structural basis of cADPR isomer selectivity by ThsA and demonstrate that v2-cADPR (3′cADPR) activates the NADase function of ThsA by changing its tetramer organization.

Immunity suppression by HopAM1 requires v2-cADPR (3′cADPR) production

3′cADPR (v2-cADPR) is also produced by the *P. syringae* DC3000 effector HopAM1 (*21*). To examine HopAM1's ability to suppress immunity, we generated transgenic *Arabidopsis* plants that express HopAM1 and the catalytically null mutant $HopAM1^{E191A}$. The transgenic plants were challenged with the immunity-inducing peptide flg22, and the production of reactive oxygen species (ROS), a hallmark of plant immunity, was quantified. Plants induced to express HopAM1 with estradiol, but not $HopAM1^{E191A}$ or the uninduced plants, showed suppressed ROS production (Fig. 6A). The immunity suppression of HopAM1 correlates with v2-cADPR (3′cADPR) production but not NAD^+ depletion (Fig. 6B).

Arabidopsis FRK1 (flg22-induced receptor-like kinase 1) is rapidly induced by multiple microbe-associated molecular patterns, and *FRK1* promoter luciferase reporter (*FRK1-LUC*) lines provide a dynamic readout of pathogen suppression of pattern-triggered immunity (*36*). Real-time imaging of DC3000 or DC3000Δ*hopAM1-1/1-2* challenged *FRK1-LUC* plants shows faster suppression of luciferase activity in DC3000 compared with the HopAM1 mutant (Fig. 6C). Fv/Fm, the maximum (dark-adapted) quantum efficiency of photosystem II, is a chlorophyll fluorescence parameter that allows nondestructive quantitative and spatial measurements of plant health. Fv/Fm has been shown to be strongly suppressed by virulent DC3000 (*36*), the extent of which is modulated by effective pattern-triggered immunity (*37*). Consistent with the reduced suppression of FRK1-LUC luciferase activity in *FRK1-LUC* plants, suppression of Fv/Fm was reduced after infection with the DC3000Δ*hopAM1-1/1-2* mutant (Fig. 6, D and E), and these immunity suppression phenotypes are directly linked to the production of v2-cADPR (3′cADPR; Fig. 6, F to I). These results indicate that v2-cADPR (3′cADPR) is responsible for HopAM1's suppression of plant immunity (a speculative model is shown in fig. S13).

Because HopAM1 acts in plant cells, we also tested its 2′,3′-cAMP and 2′,3′-cGMP synthetase activity, either as a recombinant protein with DNA as a substrate or in *Arabidopsis* challenged with DC3000 or DC3000Δ*hopAM1-1/1-2* (fig. S14). In neither case could we detect any production of 2′,3′-cAMP, cGMP, cyclic cytidine triphosphate (cCTP), or cyclic uridine triphosphate (cUTP).

Discussion

Bacterial and plant TIR domains produce cyclic signaling nucleotides with immune and virulence functions using NAD^+ or nucleic acids as substrates (*14*, *15*, *21*, *22*, *26*, *32*, *33*, *38*–*40*). Here, we report the chemical structures of two TIR domain–produced cADPR isomers, v-cADPR and v2-cADPR, which reveal that TIR domains can catalyze O-glycosidic bond formation between the ribose sugars in ADPR and that cyclization occurs at the 2′ (v-cADPR; 2′cADPR) and 3′ (v2-cADPR; 3′cADPR) positions of the adenosine ribose. These linkages differ from the canonical cADPR (produced by glycohydrolases such as CD38, *Aplysia californica* ADP-ribosyl cyclase, and the SARM1 TIR domain),

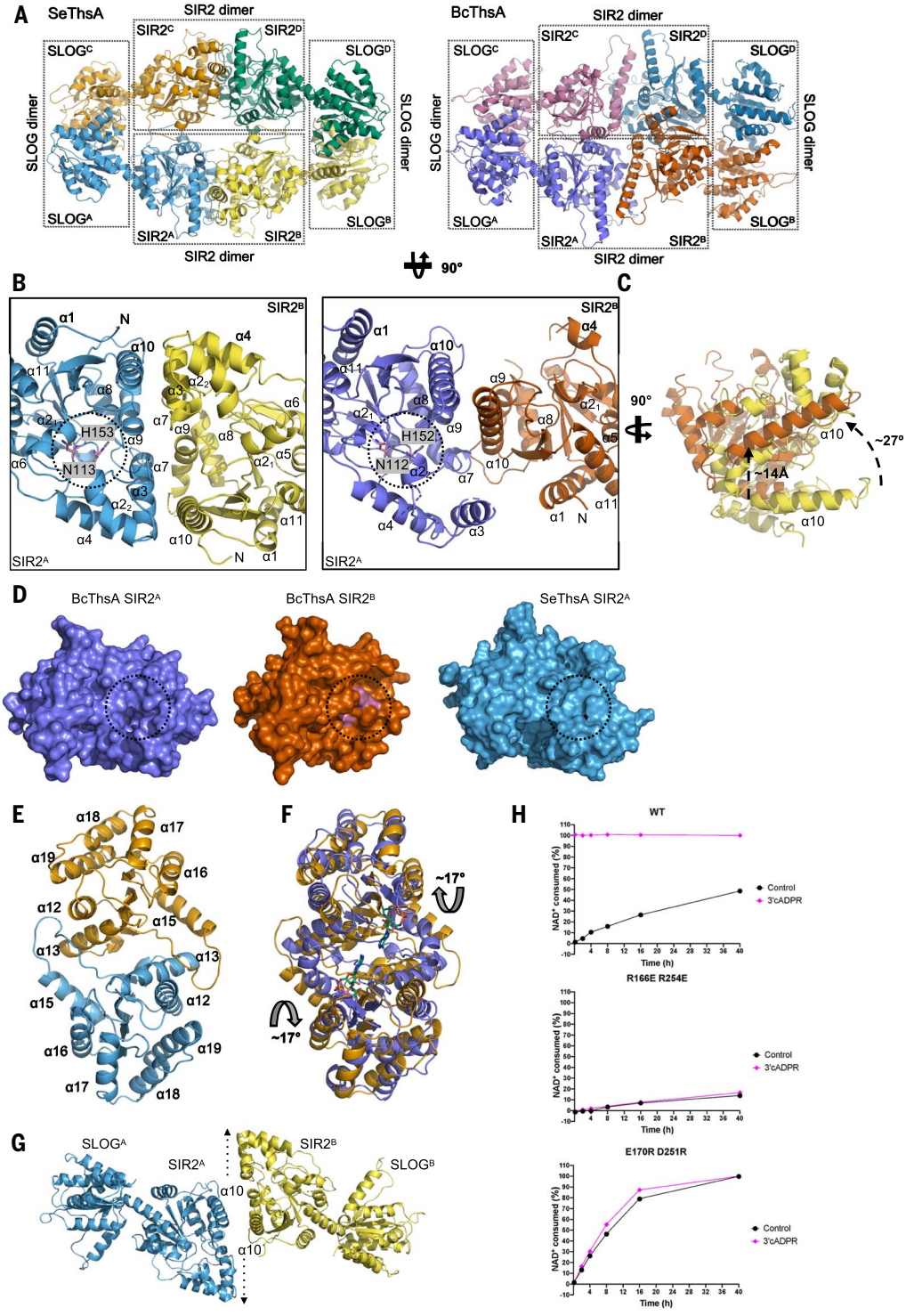

Fig. 5. 3′cADPR (v2-cADPR) changes ThsA tetramer organization.
(**A**) Structure of SeThsA (left; chains colored in sky blue, yellow, orange, and green) and BcThsA (right; chains colored in slate, red, magenta, and blue) tetramers. SLOG and SIR2 dimers are highlighted by dashed black boxes. (**B**) Enlarged cutaways of SeThsA (left) and BcThsA (right) SIR2 dimers. Dashed circles represent active site regions with catalytically important residues (N113 and H153 in SeThsA; N112 and H152 in BcThsA) displayed in stick representation (magenta). SIR2 dimers were superimposed using $SIR2^A$ of SeThsA and BcThsA. (**C**) Comparison of $SIR2^B$ in superimposed SeThsA and BcThsA SIR2 dimers. Movement of BcThsA $SIR2^B$ (salmon) with respect to the SeThsA $SIR2^B$ (yellow) is indicated by the black dashed arrows. (**D**) Surface representation of ThsA SIR2 domains. The dashed circles indicate the catalytic residues (magenta). (**E**) SeThsA SLOG dimer. (**F**) Structural superposition of SeThsA (orange) and BcThsA (slate) SLOG dimers. Movements of BcThsA SLOG domains with respect to the SeThsA SLOG domains are indicated by gray arrows. (**G**) Predicted model of SeThsA after 3′cADPR binding. Dashed arrows indicate the direction of SeThsA SIR2 domain movements induced by v2-cADPR (3′cADPR) binding to the SLOG domains. (**H**) NADase activities of 50 μM SeThsA mutants ± 50 μM 3′cADPR. Initial NAD^+ concentration was 500 μM.

which is cyclized via the N1 position of the adenine ring (*16*, *18*, *41*) and do not involve the alternative N positions (N6 and N7) of the adenine ring (*15*, *21*). NAD^+-dependent O-glycosidic bond formation between ribose sugars is a new enzymatic activity of TIR domains, but it has been reported for the ADP-ribosyl transferase (ART) domain of poly(ADP-ribose) polymerases (PARPs), which catalyze 2′–1″ and 2″–1″ ribose-ribose bonds between ADPR molecules using NAD^+ as a substrate (*42*, *43*).

NADase activity of SARM1 and plant TIR domains requires self-association (*13*, *14*, *25*), and our biochemical studies with AbTir suggest that this is also the case for cADPR isomer–producing bacterial TIR domains. The CC domains of both AbTir and TcpB (*27*) self-associate in solution and may therefore have a similar role to SARM1 SAM domains, plant TNL NB-ARC domains, and bacterial SAVED (*44*) and STING (*45*) domains in facilitating TIR-domain clustering.

Crystal structures of cADPR isomer–producing bacterial TIR domains $AbTir^{TIR}$, $BtTir^{TIR}$, $TcpB^{TIR}$ (*27*, *29*, *30*), and BcThsB (*23*) do not display interfaces analogous to enzyme and scaffold TIR-domain assemblies (*3*). Our cryo-EM structure of

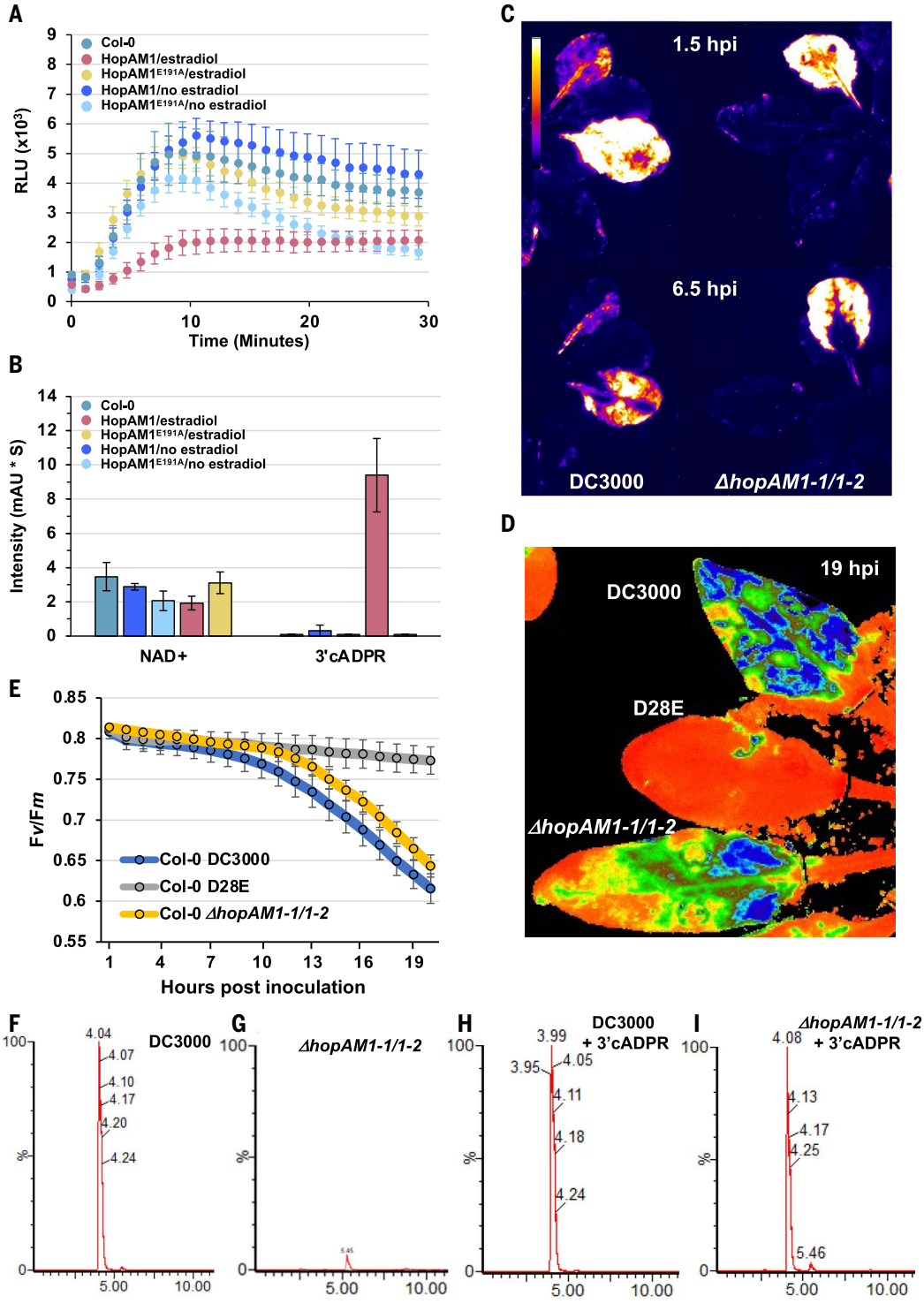

Fig. 6. 3′cADPR (v2-cADPR) production and immunity suppression by HopAM1. (**A**) ROS production of *Arabidopsis* transgenic plants expressing the *P. syringae* DC3000 effector HopAM1 or HopAM1^{E191A}, induced with 10 μM estradiol. ROS production was induced with 1 μM flg22. Data are presented as means ± SE (n = 12; Student's t test, $p < 0.01$). RLU, luminescence unit. (**B**) Quantification of NAD$^+$ and 3′cADPR from transgenic leaf samples in (A). Data are presented as means ± SE (n = 3). Transgenic plants expressing HopAM1 (estradiol-induced) produce significantly lower levels of ROS and significantly higher amounts of 3′cADPR, whereas the differences in NAD$^+$ levels are not significant (Student's t test; $p < 0.01$). mAU, milli–absorbance unit. (**C**) Suppression of pattern-triggered immunity measured by *FRK1-LUC* activity after challenge with DC3000 or the DC3000Δ*hopAM1-1/1-2* mutant. hpi, hours postinoculation. (**D**) Representative chlorophyll fluorescence images of Fv/Fm, a nondestructive measurement related to photosynthetic activity that relates to plant health, after challenge with DC3000, the Δ*hopAM1-1/1-2* mutant, or the effector-deficient mutant DC3000 D28E (reporting pattern triggered immunity). (**E**) The respective quantitative Fv/Fm measurements over the infection time course in (D). Error bars represent SE between three biological replicates of the same challenge, with the Δ*hopAM1-1/1-2* mutant being significantly different from DC3000 (Student's t test, $p < 0.05$ from 18 hpi). The graph is representative of four independent experiments. (**F** to **I**) LC-MS/MS analysis at 18 hpi of v2-cADPR (3′cADPR) production in *A. thaliana* Col-0 challenged with virulent DC3000 (F) or the Δ*hopAM1-1/1-2* mutant (G) and the respective spectra when co-injected with v2-cADPR (3′cADPR) standard from AaTir^{TIR} [(H) and (I)]. The retention time (x axis) is reported in minutes; the y axis reports the relative count per second (with 100% corresponding to the most intense peak). All leaves were challenged with an inoculum of OD_{600nm} (optical density at 600 nm) of 0.15.

the filamentous assembly of AbTir^{TIR}:3AD reveals a scaffold assembly arrangement analogous to MAL and MyD88 (*5*, *7*). Our mutagenesis data confirm that the observed arrangement is important for its catalytic function and that an intact BB loop is required. The active site is similar to the one in SARM1 (*25*), consistent with it being formed though the analogous BE interface–mediated association. Conformational changes in AbTir^{TIR} monomers are required to form the filamentous assembly. Future studies will define how additional domains in bacterial TIR proteins facilitate the active configuration and what size active complexes form in bacterial cells. The symmetric interface—found in crystal structures of all bacterial TIR domain-containing proteins with known structure, except for BcThsB (*23*, *27*–*30*), and shown to facilitate TcpB self-association and modulation of Toll-like receptor signaling (*27*, *46*)—may play a regulatory role in the transition to the active state.

A highly conserved tryptophan residue in the αC helical region, part of the previously

defined WXXXE motif (*47*) (where X is any residue), plays a role in the cyclization of ADPR by bacterial TIR domains. The equivalent tryptophan also plays a role in the catalytic activity by SARM1 and plant TIR domains. In SARM1, this tryptophan (W638) mediates aromatic stacking interactions with NAD^+ mimetics and the W638A mutation reduces NADase activity (*13*, *25*). In the flax L6 TNL protein, alanine mutation of the equivalent tryptophan (W131) abrogates cell-death signaling, and, in the cryo-EM structure of the related flax L7 TIR domain in complex with DNA, it is involved in interaction with the product 2′,3′-cAMP (*26*, *48*). In the *A. californica* ADP ribose cyclase, related to CD38 and similar to AbTir and AaTir in that it produces a cyclic ADPR (canonical cADPR) as the major product of NAD^+ hydrolysis, a phenylalanine residue (F174) directs the folding of the substrate during the cyclization reaction by interacting with the adenine base of ADPR after nicotinamide cleavage (*49*, *50*). Cyclization of 1″-2′ and 1″-3′ ribose O-glycosidic bonds in ADPR by TIR domains will require the two ribose sugars to come into proximity after nicotinamide cleavage and a possible role for the conserved tryptophan residue is to facilitate such substrate folding through interaction with the adenine base.

Although multiple plant TNL proteins and bacterial TIR proteins produce cADPR isomers, their mechanism of action and targets are only starting to be resolved. We speculate that the ThsB-produced cADPR isomer of the Thoeris defense system (*22*) corresponds to v2-cADPR (3′cADPR) because this isomer is a strong activator of ThsA NADase activity and has nanomolar affinity for ThsA proteins from different bacteria (Fig. 4). 2′cADPR (v-cADPR) can also trigger the NADase activity of ThsA [Fig. 4B and (*22*)], but a higher concentration is needed to activate ThsA because it shows weaker binding than v2-cADPR (3′cADPR). Consistent with our biochemical data, the $BcThsA^{SLOG}$:v2-cADPR (3′cADPR) complex structure reveals that the binding pocket is selective for v2-cADPR (3′ cADPR), which induces a reorganization of the ThsA tetramer to allosterically promote binding to its substrate NAD^+. This mode of action is reminiscent of the NMN-induced activation of SARM1, which is only able to bind and cleave the substrate NAD^+ after a change to its octamer organization triggered by NMN binding to its ARM domain (*25*). 2′cADPR (v-cADPR) produced by the protein BdTIR from the plant *Brachipodium distachyon* has been found to bind to the protein Thoeris anti-defense 1 (Tad1) that inhibits Thoeris immunity (*51*), but there is no data showing that this is the isomer produced by ThsB proteins. Future studies will determine the identity of ThsB-produced cADPR isomers, the structural basis for how they activate ThsA, and whether SLOG domains in cytokinin-activating proteins in plants (*52*, *53*) are also receptors for cADPR isomers.

The nucleotides pRib-AMP and pRib-ADP [2′-(5″-phosphoribosyl)-5′-adenosine monophosphate and 2′-(5″-phosphoribosyl)-5′-adenosine diphosphate] were shown to trigger immune signaling in plants by allosterically promoting the EDS1 (enhanced disease susceptibility 1)–PAD4 (phytoalexin deficient 4) complex to bind to the plant NLR protein ADR1-L1; the production requires TIR proteins (*32*). Plant TIR domains can also generate ADP-ribosylated ATP (ADPr-ATP) and di-ADPR, which in turn promote the association of EDS1 and SAG101 (senescence-associated gene 101) with the helper NLR NRG1A (N requirement gene 1A) (*33*). Multiple TIR domains produce cADPR isomers in plants, but the EDS1-binding molecules have not yet been detected in planta and their biosynthetic pathways are not defined. The authors of (*32*, *33*) proposed a pathway for the production of pRib-AMP and pRib-ADP as well as ADPr-ATP and di-ADPR that does not involve cADPR isomers. Our cADPR isomer structures show that pRib-AMP can be derived directly from v-cADPR (2′cADPR) by cleavage of its pyrophosphate bond, suggesting that NAD^+ could be the substrate in this case. The cleavage of the pyrophosphate bond could indicate the involvement of plant NUDIX hydrolases like NUDX6 and 7, which regulate plant immunity by degrading 2′,3′-cAMP and 2′,3′-cGMP, the other nucleotides putatively produced by TIR domains (*26*).

3′-*O*-β-D-ribofuranosyladenosine, which has an identical 1″-3′ O-glycosidic linkage to v2-cADPR (3′cADPR) but lacks the phosphate groups, has been shown to accumulate in leaves infected with the HopAM1-producing bacterium *P. syringae* DC3000 (*54*), suggesting that cADPR isomers can be further modified in plants. Pyrophosphate bond cleavage of HopAM1-produced v2-cADPR (3′cADPR), followed by removal of the two ribose-5-phosphate groups, is a possible synthetic path for this nucleotide product, which suggests that cADPR isomers perhaps not only serve as signaling molecules but are also important intermediates in the synthesis of additional previously uncharacterized nucleosides associated with plant immunity. In conclusion, our study unravels the cyclization site of cADPR isomers and informs on their production by TIR domains and their signaling in immunity pathways in bacteria and plants.

Methods summary

A comprehensive description of materials and methods is presented in the supplementary materials. These descriptions include the details of cloning of expression plasmids and side-directed mutagenesis, protein expression and purification, different assays of NAD^+ cleavage and characterization of its products (fluorescence, NMR, HPLC, and mass spectrometry-based approaches), and bioinformatic analysis. For the determination of chemical structures of cADPR isomers, the compounds were produced by AbTir, AaTir, and HopAM1 and the structures were determined using NMR (assignments are provided in tables S2 to S4) and liquid chromatography–tandem mass spectrometry (LC-MS/MS). Protein:ligand and protein:protein interactions were characterized by STD NMR, ITC, and SEC-MALS. Three-dimensional structures were determined using x-ray crystallography (crystallographic parameters are provided in table S5) and cryo-EM (structure determination details are provided in fig. S5 and table S6). Also described are phytobacterial challenge and ROS assays in HopAM1-expressing *Arabidopsis* plants.

REFERENCES AND NOTES

1. T. Ve, S. J. Williams, B. Kobe, Structure and function of Toll/interleukin-1 receptor/resistance protein (TIR) domains. *Apoptosis* **20**, 250–261 (2015). doi: 10.1007/s10495-014-1064-2; pmid: 25451009
2. S. Nimma, T. Ve, S. J. Williams, B. Kobe, Towards the structure of the TIR-domain signalosome. *Curr. Opin. Struct. Biol.* **43**, 122–130 (2017). doi: 10.1016/j.sbi.2016.12.014; pmid: 28092811
3. S. Nimma *et al*., Structural evolution of TIR-domain signalosomes. *Front. Immunol.* **12**, 784484 (2021). doi: 10.3389/fimmu.2021.784484; pmid: 34868065
4. N. Maruta *et al*., Structural basis of NLR activation and innate immune signalling in plants. *Immunogenetics* **74**, 5–26 (2022). doi: 10.1007/s00251-021-01242-5; pmid: 34981187
5. M. T. B. Clabbers *et al*., MyD88 TIR domain higher-order assembly interactions revealed by microcrystal electron diffraction and serial femtosecond crystallography. *Nat. Commun.* **12**, 2578 (2021). doi: 10.1038/s41467-021-22590-6; pmid: 33972532
6. P. R. Vajjhala, T. Ve, A. Bentham, K. J. Stacey, B. Kobe, The molecular mechanisms of signaling by cooperative assembly formation in innate immunity pathways. *Mol. Immunol.* **86**, 23–37 (2017). doi: 10.1016/j.molimm.2017.02.012; pmid: 28249680
7. T. Ve *et al*., Structural basis of TIR-domain-assembly formation in MAL- and MyD88-dependent TLR4 signaling. *Nat. Struct. Mol. Biol.* **24**, 743–751 (2017). doi: 10.1038/nsmb.3444; pmid: 28759049
8. R. R. Rana, M. Zhang, A. M. Spear, H. S. Atkins, B. Byrne, Bacterial TIR-containing proteins and host innate immune system evasion. *Med. Microbiol. Immunol. (Berl.)* **202**, 1–10 (2013). doi: 10.1007/s00430-012-0253-2; pmid: 22772799
9. S. Doron *et al*., Systematic discovery of antiphage defense systems in the microbial pangenome. *Science* **359**, eaar4120 (2018). doi: 10.1126/science.aar4120; pmid: 29371424
10. B. R. Morehouse *et al*., STING cyclic dinucleotide sensing originated in bacteria. *Nature* **586**, 429–433 (2020). doi: 10.1038/s41586-020-2719-5; pmid: 32877915
11. N. Tal *et al*., Cyclic CMP and cyclic UMP mediate bacterial immunity against phages. *Cell* **184**, 5728–5739.e16 (2021). doi: 10.1016/j.cell.2021.09.031; pmid: 34644530
12. B. Koopal *et al*., Short prokaryotic Argonaute systems trigger cell death upon detection of invading DNA. *Cell* **185**, 1471–1486.e19 (2022). doi: 10.1016/j.cell.2022.03.012; pmid: 35381200
13. S. Horsefield *et al*., NAD^+ cleavage activity by animal and plant TIR domains in cell death pathways. *Science* **365**, 793–799 (2019). doi: 10.1126/science.aax1911; pmid: 31439792
14. L. Wan *et al*., TIR domains of plant immune receptors are NAD^+-cleaving enzymes that promote cell death. *Science* **365**, 799–803 (2019). doi: 10.1126/science.aax1771; pmid: 31439793
15. K. Essuman *et al*., TIR domain proteins are an ancient family of NAD^+-consuming enzymes. *Curr. Biol.* **28**, 421–430.e4 (2018). doi: 10.1016/j.cub.2017.12.024; pmid: 29395922
16. K. Essuman *et al*., The SARM1 Toll/interleukin-1 receptor domain possesses intrinsic NAD^+ cleavage activity that promotes pathological axonal degeneration. *Neuron* **93**,

1334–1343.e5 (2017). doi: 10.1016/j.neuron.2017.02.022; pmid: 28334607
17. M. D. Figley *et al*., SARM1 is a metabolic sensor activated by an increased NMN/NAD^+ ratio to trigger axon degeneration. *Neuron* **109**, 1118–1136.e11 (2021). doi: 10.1016/j.neuron.2021.02.009; pmid: 33657413
18. H. C. Lee, R. Aarhus, D. Levitt, The crystal structure of cyclic ADP-ribose. *Nat. Struct. Biol.* **1**, 143–144 (1994). doi: 10.1038/nsb0394-143; pmid: 7656029
19. Z. Duxbury *et al*., Induced proximity of a TIR signaling domain on a plant-mammalian NLR chimera activates defense in plants. *Proc. Natl. Acad. Sci. U.S.A.* **117**, 18832–18839 (2020). doi: 10.1073/pnas.2001185117; pmid: 32709746
20. J. M. Coronas-Serna *et al*., The TIR-domain containing effectors BtpA and BtpB from *Brucella abortus* impact NAD metabolism. *PLOS Pathog.* **16**, e1007979 (2020). doi: 10.1371/journal.ppat.1007979; pmid: 32298382
21. S. Eastman *et al*., A phytobacterial TIR domain effector manipulates NAD^+ to promote virulence. *New Phytol.* **233**, 890–904 (2022). doi: 10.1111/nph.17805; pmid: 34657283
22. G. Ofir *et al*., Antiviral activity of bacterial TIR domains via immune signalling molecules. *Nature* **600**, 116–120 (2021). doi: 10.1038/s41586-021-04098-7; pmid: 34853457
23. D. Ka, H. Oh, E. Park, J. H. Kim, E. Bae, Structural and functional evidence of bacterial antiphage protection by Thoeris defense system via NAD^+ degradation. *Nat. Commun.* **11**, 2816 (2020). doi: 10.1038/s41467-020-16703-w; pmid: 32499527
24. A. M. Burroughs, L. Aravind, Identification of uncharacterized components of prokaryotic immune systems and their diverse eukaryotic reformulations. *J. Bacteriol.* **202**, e00365–e00320 (2020). doi: 10.1128/JB.00365-20; pmid: 32868406
25. Y. Shi *et al*., Structural basis of SARM1 activation, substrate recognition, and inhibition by small molecules. *Mol. Cell* **82**, 1643–1659.e10 (2022). doi: 10.1016/j.molcel.2022.03.007; pmid: 35334231
26. D. Yu *et al*., TIR domains of plant immune receptors are 2′,3′-cAMP/cGMP synthetases mediating cell death. *Cell* **185**, 2370–2386.e18 (2022). doi: 10.1016/j.cell.2022.04.032; pmid: 35597242
27. M. Alaidarous *et al*., Mechanism of bacterial interference with TLR4 signaling by *Brucella* Toll/interleukin-1 receptor domain-containing protein TcpB. *J. Biol. Chem.* **289**, 654–668 (2014). doi: 10.1074/jbc.M113.523274; pmid: 24265315
28. S. L. Chan *et al*., Molecular mimicry in innate immunity: Crystal structure of a bacterial TIR domain. *J. Biol. Chem.* **284**, 21386–21392 (2009). doi: 10.1074/jbc.C109.007591; pmid: 19535337
29. B. Kaplan-Türköz *et al*., Structure of the Toll/interleukin 1 receptor (TIR) domain of the immunosuppressive *Brucella* effector BtpA/Btp1/TcpB. *FEBS Lett.* **587**, 3412–3416 (2013). doi: 10.1016/j.febslet.2013.09.007; pmid: 24076024
30. G. A. Snyder *et al*., Crystal structures of the Toll/Interleukin-1 receptor (TIR) domains from the *Brucella* protein TcpB and host adaptor TIRAP reveal mechanisms of molecular mimicry. *J. Biol. Chem.* **289**, 669–679 (2014). doi: 10.1074/jbc.M113.523407; pmid: 24275656
31. J. S. Weagley *et al*., Products of gut microbial Toll/interleukin-1 receptor domain NADase activities in gnotobiotic mice and Bangladeshi children with malnutrition. *Cell Rep.* **39**, 110738 (2022). doi: 10.1016/j.celrep.2022.110738; pmid: 35476981
32. A. Jia *et al*., TIR-catalyzed ADP-ribosylation reactions produce signaling molecules for plant immunity. *Science* **377**, eabq8180 (2022). doi: 10.1126/science.abq8180; pmid: 35857644
33. S. Huang *et al*., Identification and receptor mechanism of TIR-catalyzed small molecules in plant immunity. *Science* **377**, eabq3297 (2022). doi: 10.1126/science.abq3297; pmid: 35857645
34. S. Ma *et al*., Direct pathogen-induced assembly of an NLR immune receptor complex to form a holoenzyme. *Science* **370**, eabe3069 (2020). doi: 10.1126/science.abe3069; pmid: 33273071
35. R. Martin *et al*., Structure of the activated ROQ1 resistosome directly recognizing the pathogen effector XopQ. *Science* **370**, eabd9993 (2020). doi: 10.1126/science.abd9993; pmid: 33273074
36. M. de Torres Zabala *et al*., Chloroplasts play a central role in plant defence and are targeted by pathogen effectors. *Nat. Plants* **1**, 15074 (2015). doi: 10.1038/nplants.2015.74; pmid: 27250009
37. S. Breen *et al*., Chloroplasts play a central role in facilitating MAMP-triggered immunity, pathogen suppression of immunity and crosstalk with abiotic stress. *Plant Cell Environ.*pce.14408 (2022). doi: 10.1111/pce.14408; pmid: 35892221
38. M. T. Hulin, W. Ma, Pangenomics facilitated with structural analysis reveals host NAD^+ manipulation as a major virulence activity of bacterial effectors. bioRxiv 2022.2006.2007.495176 [Preprint] (2022); doi: 10.1101/2022.06.07.495176
39. S. Eastman, A. Bayless, M. Guo, The nucleotide revolution: Immunity at the intersection of TIR-domains, nucleotides, and Ca^2. *Mol. Plant Microbe Interact.*MPMI-06-22-0132-CR (2022). doi: 10.1094/MPMI-06-22-0132-CR; pmid: 35881867
40. K. Essuman, J. Milbrandt, J. L. Dangl, M. T. Nishimura, Shared TIR enzymatic functions regulate cell death and immunity across the tree of life. *Science* **377**, eabo0001 (2022). doi: 10.1126/science.abo0001; pmid: 35857622
41. M. Howard *et al*., Formation and hydrolysis of cyclic ADP-ribose catalyzed by lymphocyte antigen CD38. *Science* **262**, 1056–1059 (1993). doi: 10.1126/science.8235624; pmid: 8235624
42. L. Aravind, D. Zhang, R. F. de Souza, S. Anand, L. M. Iyer, The natural history of ADP-ribosyltransferases and the ADP-ribosylation system. *Curr. Top. Microbiol. Immunol.* **384**, 3–32 (2015). doi: 10.1007/82_2014_414; pmid: 25027823
43. K. Ueda, O. Hayaishi, ADP-ribosylation. *Annu. Rev. Biochem.* **54**, 73–100 (1985). doi: 10.1146/annurev.bi.54.070185.000445; pmid: 3927821
44. G. Hogrel *et al*., Cyclic nucleotide-induced helical structure activates a TIR immune effector. *Nature* **608**, 808–812 (2022). doi: 10.1146/annurev.bi.54.070185.000445; pmid: 3927821
45. B. R. Morehouse *et al*., Cryo-EM structure of an active bacterial TIR-STING filament complex. *Nature* **608**, 803–807 (2022). doi: 10.1038/s41586-022-04999-1; pmid: 35859168
46. A. Chaudhary *et al*., The *Brucella* TIR-like protein TcpB interacts with the death domain of MyD88. *Biochem. Biophys. Res. Commun.* **417**, 299–304 (2012). doi: 10.1016/j.bbrc.2011.11.104; pmid: 22155231
47. C. Felix *et al*., The *Brucella* TIR domain containing proteins BtpA and BtpB have a structural WxxxE motif important for protection against microtubule depolymerisation. *Cell Commun. Signal.* **12**, 53 (2014). doi: 10.1186/s12964-014-0053-y; pmid: 25304327
48. M. Bernoux *et al*., Structural and functional analysis of a plant resistance protein TIR domain reveals interfaces for self-association, signaling, and autoregulation. *Cell Host Microbe* **9**, 200–211 (2011). doi: 10.1016/j.chom.2011.02.009; pmid: 21402359
49. Q. Liu *et al*., Structural basis for enzymatic evolution from a dedicated ADP-ribosyl cyclase to a multifunctional NAD hydrolase. *J. Biol. Chem.* **284**, 27637–27645 (2009). doi: 10.1074/jbc.M109.031005; pmid: 19640846
50. R. Graeff *et al*., Mechanism of cyclizing NAD to cyclic ADP-ribose by ADP-ribosyl cyclase and CD38. *J. Biol. Chem.* **284**, 27629–27636 (2009). doi: 10.1074/jbc.M109.030965; pmid: 19640843
51. A. Leavitt *et al*., Viruses inhibit TIR gcADPR signaling to overcome bacterial defense. bioRxiv 2022.2005.2003.490397 [Preprint] (2022); https://doi.org/10.1101/2022.05.03.490397.
52. A. M. Burroughs, D. Zhang, D. E. Schäffer, L. M. Iyer, L. Aravind, Comparative genomic analyses reveal a vast, novel network of nucleotide-centric systems in biological conflicts, immunity and signaling. *Nucleic Acids Res.* **43**, 10633–10654 (2015). doi: 10.1093/nar/gkv1267; pmid: 26590262
53. T. Kuroha *et al*., Functional analyses of *LONELY GUY* cytokinin-activating enzymes reveal the importance of the direct activation pathway in *Arabidopsis*. *Plant Cell* **21**, 3152–3169 (2009). doi: 10.1105/tpc.109.068676; pmid: 19837870
54. M. S. Drenichev *et al*., A role for 3′-O-β-D-ribofuranosyladenosine in altering plant immunity. *Phytochemistry* **157**, 128–134 (2019). doi: 10.1016/j.phytochem.2018.10.016; pmid: 30399495

ACKNOWLEDGMENTS

We acknowledge use of the Australian Synchrotron MX facility and thank the staff for their support. We acknowledge the Centre for Microscopy and Microanalysis, University of Queensland (UQ), and staff (L. Brillault, M. Floetenmeyer, R. Webb, and R. Wepf). We thank F. Makino (JEOL) for help with cryo-EM data collection; K. Arachchige and J. Clegg (UQ) for help with crystallization; F. Rose (Griffith University) for help with HPLC purification of 2′cADPR and 3′cADPR; and M. Mobli (UQ) for advice on NMR. **Funding:** The work was supported by the National Health and Medical Research Council (NHMRC) (grants 1196590 to T.V., 1107804 and 1160570 to B.K. and T.V., 1071659 to B.K., and 1108859 to T.V.); an Australian Research Council (ARC) Future Fellowship (FT200100572 to T.V.); an ARC Laureate Fellowship (FL180100109 to B.K.); an ARC Discovery Early Career Researcher Award (DE170100783 to T.V.); the National Institutes of Health (R01NS087632 to J.M. and A.D.); and the Biotechnology and Biological Sciences Research Council (BB/V00400X/1 to M.Gr. and L.S.). Y.S. was a recipient of a Griffith University Postdoctoral Fellowship Scheme. Nebraska Soybean Board project no. 1734 funded the research assistantship for S.E. **Author contributions:** Conceptualization: M.K.M., Y.S., M.A.Z., M.Gr., M.Gu., J.M., A.D., T.V., B.K.; Investigation: M.K.M., Y.S., S.L., M.A.Z., N.D., S.E., T.G.S., W.G., V.M., T.M., J.S.W., S.J.H., E.V., L.H.-T., N.M., B.Y.J.L., H.B., M.J.L., I.P., N.K., L.S., M.Gr., J.D.N., M.Gu., T.V.; Writing – original draft: M.K.M., Y.S., S.L., T.V., B.K.; Writing – review and editing: All authors; Funding acquisition: T.V., B.K., M.Gu., M.Gr., L.S., J.M., A.D.; Resources: T.V., B.K., J.M., A.D.; Supervision: T.V., B.K., J.D.N., J.M., A.D., M.A.S., M.Gr., M.Gu. **Competing interests:** The authors have no competing interests. **Data and materials availability:** Coordinates and structure factors for the $AbTir^{TIR}$, $BtTir^{TIR}$, $BcThsA^{SLOG}$:v2-cADPR (3′cADPR), and SeThsA crystal structures have been deposited in the Protein Data Bank with IDs 7UWG, 7UXR, 7UXS, and 7UXT, respectively. Maps and coordinates for the $AbTir^{TIR}$:3AD cryo-EM structure have been deposited to the Electron Microscopy Data Bank (EMD-26862) and Protein Data Bank (7UXU), respectively. All other data are in the main paper or supplementary materials. Some specific reagents such as 2′cADPR and 3′cADPR may be available from the corresponding authors with a completed materials transfer agreement; restrictions may apply because of limited availability and prioritization for internal use.

SUPPLEMENTARY MATERIALS

science.org/doi/10.1126/science.adc8969
Materials and Methods
Figs. S1 to S14
Tables S1 to S9
References (*55*–*85*)
MDAR Reproducibility Checklist
Movies S1 to S3
Data S1 to S4

View/request a protocol for this paper from *Bio-protocol*.

Submitted 8 May 2022; accepted 23 August 2022
Published online 1 September 2022
10.1126/science.adc8969